Al 3+ Additive in the Nickel Hydroxide Obtained by High-Temperature Two-Step Synthesis: Activator or Poisoner for Chemical Power Source Application?

V. V. Kovalenko, V. Kotok, A. Sykchin, B. Ananchenko, A.V. Chernyad'ev,
A. Burkov, S. Deabate, A. Mehdi, F. Henn, J.-L. Bantignies, et al.

HAL Id: hal-02924352
https://hal.science/hal-02924352

Submitted on 8 Jun 2023

Al^{3+} Additive in the Nickel Hydroxide Obtained by High-Temperature Two-Step Synthesis: Activator or Poisoner for Chemical Power Source Application?

V. L. Kovalenko,[1,2,z] **V. A. Kotok,**[1,2] **A. Sykchin,**[2] **B. A. Ananchenko,**[2] **A.V. Chernyad'ev,**[2]
A. A. Burkov,[2] **S. Deabate,**[4] **A. Mehdi,**[5] **F. Henn,**[3] **J.-L. Bantignies,**[3] **K. L. Bychkov,**[9]
V.V. Verbitskiy,[6,7,8] **and K. M. Sukhyy**[1]

[1]*Ukrainian State University of Chemical Technology, Dnepr 49005, Ukraine*
[2]*Vyatka State University, Kirov, 610000, Russia*
[3]*Equipe Nanomateriaux et Spectroscopie, Laboratoire Charles Coulomb, UMR CNRS 5221, Université de Montpellier, 34090 Montpellier, France*
[4]*Institut Européen des Membranes, UMR CNRS-ENSCM-UM 5635, Université de Montpellier, 34090 Montpellier, France*
[5]*Institut Charles Gerhardt de Montpellier, UMR CNRS-UM 5253, Université de Montpellier, 34090 Montpellier, France*
[6]*Taras Shevchenko National University of Kyiv, Kyiv 01601, Ukraine*
[7]*National Ecology and Nature Center, Kyiv 04074, Ukraine*
[8]*National Pedagogical Dragomanov University, Kyiv 01601, Ukraine*
[9]*Skolkovo Institute of Science and Technology, Moscow, 121205, Russia*

Aim of investigation is to study the possibility of activating a promising Ni(OH)$_2$, prepared using two-step high-temperature synthesis, by adding 3%, 5% and 10% (mol.) Al^{3+} to Ni^{2+}. For describing the intercalation of Al^{3+} into hydroxide structure, "Separate-Solid—Liquid—Solid" mechanism, which included the formation of separate Al-containing phase on synthesis stage, and incorporation of Al^{3+} into Ni(OH)$_2$ or formation of surface compounds during hydrolysis stage, has been proposed. EDX analysis of precursor confirmed the formation of separate Al-containing phases. By means of PXRD, EDX, SEM, TEM revealed realization of both ways of Al^{3+} incorporation: at high amounts of Al^{3+} (5% and 10% mol.), predominantly surface compounds are formed with distorted and altered particle shape and appearance of "core–shell" particles. At low amounts of Al^{3+} (3% mol.), permeably doping occurs, with partial intercalation of Al^{3+} into the nickel hydroxide structure. Based on CVA and GCDC results, Al^{3+} acts as a poison upon the formation of surface compounds have been found. Upon doping of hot hydrolysis samples with aluminum, sample activation was observed, which resulted in an increase of specific capacity by 1.99 times, from 569 Fg^{-1} (pure Ni(OH)$_2$) to 1112 Fg^{-1}.

Ni(OH)$_2$, owing to its high electrochemical activity, is widely used in various electrochemical devices.[1,2] Nickel hydroxide and nickel-based LDHs are an active substance of nickel-oxide electrode in Ni-Fe, Ni-Cd, Ni-MH secondary cells.[3,4] Nickel hydroxides are also used in the Faradic electrode of hybrid supercapacitors.[5–14] For thin layer supercapacitors, a nickel hydroxide film can be formed on the conductive substrate.[15] Because oxidized form (NiOOH) of this compound has dark-brown color, while reduced form (Ni(OH)$_2$) in a thin layer is transparent, nickel hydroxide is used as electrochromic material.[16–19] Nickel hydroxide has high electrocatalytic activity and is used for electrooxidation of various organic compounds,[20,21] and in sensors.[22]

Two polymorphs of nickel hydroxides are known[23]: β-hydroxide with formula Ni(OH)$_2$ and brucite-type structure and α-hydroxide with formula 3Ni(OH)$_2$·2H$_2$O and hydrotalcite-type structure. However, paper[22] describes the formation of nickel hydroxide structure that is in-between α-form and β-form. Papers[24–26] describe the formation of hydroxide with layered ($\alpha + \beta$) structure.

α-Ni(OH)$_2$ has a high electrochemical activity. However, α-form has low stability and in concentrated alkali and at elevated temperatures it transforms into less active β-form,[27,28] results in a decrease of specific capacity. To stabilize α-form, special additives are introduced to nickel hydroxide with the formation of LDH,[29,30] which consists of the host crystal lattice with part of host hydroxide cations (Ni^{2+}) substituted by guest cations[31,32] such as Al^{3+}.[33] The extra positive charge is compensated by the incorporation of various anions that intercalated into interlayer space.[34,35] Various methods are used for α-Ni(OH)$_2$ and nickel-based LDHs preparation.[36–41] The electrochemical activity of β-Ni(OH)$_2$ is lower than α-Ni(OH)$_2$ activity, and, it possesses higher storage and cycling stability. As such, this form is preferably used in alkaline batteries and hybrid

supercapacitors.[42–45] For β-Ni(OH)$_2$ synthesis different chemical and electrochemical methods can be used.[46–48]

Because of high charge and discharge currents in the operation of the Faradic electrode of hybrid supercapacitors, the electrochemical process takes place in a particles thin surface layer. As such, special requirements for supercapacitor applicable Ni(OH)$_2$ powders include small particle size, high specific surface area, optimal crystal structure, high electrochemical activity, and cycling stability.[49–52] Requirements of high electrochemical activity and cycling stability are rather contradictory. One way to solve this contradiction is could be a synthesis of β-Ni(OH)$_2$ with special morphology increasing its activity. Such types of nickel hydroxide have simple[53,54] and ≪pseudo-simple≫ particles.[55] In previous work, we proposed an indirect two-step high-temperature synthesis. On the first stage (synthesis) sodium nickelate is formed under t = 140 °C. On the second stage, sodium nickelate is hydrolyzed under t = 170 °C. As a result, the nickel hydroxide particles with ≪pseudo-single≫ morphology, fractal geometry and the increasing specific surface have been obtained. Such type of Ni(OH)$_2$ is a promising material for supercapacitor applications. We also proposed[55] synthesis of nickel hydroxide via cold (25 °C) and hot (170 °C) hydrolysis and found that both methods result in electrochemically active nickel hydroxide samples. However, the current task is to improve the activity of these nickel hydroxide samples.

Al^{3+} is the most commonly used for the activation of nickel hydroxide. In many cases, the aluminum cation is used for stabilizing of α-Ni(OH)$_2$ with the formation of Ni-Al LDH.[35,56–64] An aluminum cation is electrochemically inert and its low atomic mass is a significant advantage. The lower molecular mass of the inert activator results in a higher content of the electrochemically active component. It is worth to note, that Al^{3+} not only stabilizes α-Ni(OH)$_2$ but also improves electrochemical activity, which means the higher specific capacity of nickel hydroxide. However, despite the introduction of Al^{3+}, the stability of α-Ni(OH)$_2$-based LDH is

insufficient, especially during cycling at high very high current densities (8C and higher). During cycling and storage, degradation of LDH can occur, leading to the release of aluminum cation into solution followed by absorption of onto nickel hydroxide. Absorbed aluminum poisons $Ni(OH)_2$, significantly reducing its electrochemical activity. As such, the activation of β-$Ni(OH)_2$ with aluminum cation is promising.[35] However, this problem has not been studied in detail.

Thus the aim of this investigation is to determine the possibility of Al^{3+} activation of β-$Ni(OH)_2$ prepared via two-step high-temperature synthesis. For this purpose, the influence of Al^{3+} on structural, morphological and electrochemical properties of β-$Ni(OH)_2$ samples have been studied.

Experimental

Samples preparation.—For experiments, commercial chemicals with analytical grade were used. The basic scheme of the synthesis[55]:

Primary stage—nickel perchlorate obtaining.—The nickel perchlorate solution was prepared according to follows: (a) addition of sodium carbonate to nickel sulfate solution under vigorous stirring with basic nickel carbonate preparation. The obtained precipitate was rinsed from sodium sulfate. The absence of sulfate ions is controlled with the negative reaction with barium nitrate; (b) an extra quantity of basic nickel carbonate reacted with 45% perchloric acid to obtain pH 6.0 ($HClO_4$ amount was calculated based on reaction stoichiometry and required mass of nickel perchlorate). The prepared solution was filtered from an extra amount of basic nickel carbonate and was evaporated to obtain the needed nickel perchlorate to water ratio.[55]

High-temperature two-step synthesis. First stage—precursor synthesis.—Required NaOH and H_2O amounts (mass ratio $NaOH:H_2O$ was 5.5:1) were put into Teflon beaker (500 ml) with a hermetically sealed lid. Beaker was heated under vigorous stirring with a magnetic Teflon stirrer to temperature 170 °C. For water loss prevention, the condenser with water flowing cooling was taking place in the hole in the beaker lid. After temperature 170 °C obtaining, prepared on the previous stage nickel perchlorate solution was drop-by drop added trough condenser. After that, the temperature was decreased to 140 °C. The first stage duration was 24 h. As a result, a sodium nickelate sediment, consists of olive-green microscale non-porous hexagonal plates, has been formed[65] according to the following reaction:

$$Ni(ClO_4)_2 + 4NaOH \rightarrow Na_2NiO_2 + 2NaClO_4 + 2H_2O \qquad [1]$$

High-temperature two-step synthesis. Second stage—precursor hydrolysis.—$Ni(OH)_2$ as a product has been obtained during hydrolysis according to the following reaction:

$$Na_2NiO_2 + 2H_2O \rightarrow Ni(OH)_2 + 2NaOH \qquad [2]$$

Hydrolysis with different temperatures was carried out[55]:

- *Hot hydrolysis.* After the sodium nickelate synthesis, mother liquor (150 ml) was recovered from the beaker, and the same water volume was added into the beaker. Then the beaker was aged 24 h under vigorous stirring with constant temperature (170 °C).
- *Cold hydrolysis.* Reaction mixture with sodium nickelate was transferred from the beaker into a big volume (5 l) of distilled water under room temperature and was aged during 24 h with stirring vigorously.

Alteration of basis scheme.—In order to study the influence of Al^{3+}, nickel hydroxide samples were synthesized with the addition of aluminum perchlorate to the solution of initial compounds (nickel perchlorate) in amounts of 3%, 5% and 10% (molar) Al^{3+} to Ni^{2+}. The samples were labeled as follows: NiAl 3% cold or NiAl 5% hot. 3%—molar content of aluminum, hot or cold—hydrolysis type.

For the synthesis of the samples with Al^{3+} addition, solutions of nickel perchlorate and aluminum perchlorate with required $Ni^{2+}:Al^{3+}$ molar ratio, have been prepared. For this, aluminum perchlorate solution was obtained by the method, similar for pure nickel perchlorate solution: a) addition of sodium carbonate to aluminum sulfate solution under vigorous stirring with precipitate formation. The obtained precipitate was rinsed from sodium sulfate. The absence of sulfate ions is controlled with the negative reaction with barium nitrate; b) an extra quantity of aluminum base carbonate reacted with 45% perchloric acid to obtain pH 6.0 ($HClO_4$ amount was calculated based on reaction stoichiometry and required mass of aluminum perchlorate). The prepared solution was filtered from an extra amount of aluminum base carbonate. After preparation, aluminum and nickel perchlorate solutions were mixed and mixed solution was evaporated to obtain the required nickel perchlorate to water ratio.

After the hydrolysis stage, $Ni(OH)_2$ sample has been filtered from the mother liquor, dried under 90 °C during 24 h, washed from soluble salts and re-dried at the same conditions.

In order to study the possible mechanism of aluminum influences, for sample NiAl 10% the synthesis procedure was interrupted on the precursor synthesis stage. The obtained precursor was vacuum filtered using a pre-heated glass frit filter, washed with isopropyl alcohol from an excess of alkali and dried at 90 °C. The sample was labeled as NiAl 10% precursor.

Samples characterization.—The crystal structure has been investigated by PXRD method with using DRON-3 diffractometer (Co-Kα radiation (wavelength 1.7903000 Å), 2θ range 10°–90°, scan rate 0.1°s^{-1}). Samples of Ni hydroxide, obtained by high-temperature two-step synthesis without Al^{3+} additive (labeled as Ni Pure Cold and Ni-Pure Hot), have been used as the referent samples for PXRD investigation. For phases detection Match! software was used. Crystallinity was calculated by Sherrer's formula. The morphology of the particles has been characterized by SEM (using microscope JEOL JSM-6510LV, Japan) and TEM (using microscope JEOL JEM-2100, Japan). The chemical composition of samples was investigated by EDX analysis with a microscope Hitachi S4500, Japan.

TG analysis has been carried out with DTG-60 ("Shimadzu," Japan) and DSC has been carried out with DSC-60 ("Shimadzu," Japan). Analysis conditions: an air atmosphere, the heating rate of 5 °Cmin^{-1}.

Electrochemical properties have been characterized by cycling voltammetry (CVA) and galvanostatic charge-discharge cycling (CDC), using SEC-2 special cell and electronic potentiostat-galvanostat Ellins P-8. For both investigations, electrodes for these electrochemical measurements were prepared by pasting of active mass on the working electrode, made from nickel foam base[82] and Ni foil current collector.[66,67] The active mass consists of a mixture of 82.5% (wt.) $Ni(OH)_2$ sample, 16%(wt.) graphite and 1.5% (wt.) PTFE.[66] The electrolyte − 6 M KOH solution. As the counter electrode a nickel grid was used and as the reference electrode –saturated SCE.CVs were recorded at potential range 0–500 mV in the two regimes: 1) single-speed mode—at 1 mVs^{-1}; 2) multispeed mode—at 1, 2, 5, 10 and 50 mVs^{-1}. Potentials in CV curves have been recalculated from SCE to NHE. Charge-discharge cycling in the supercapacitor mode has been carried out at 5, 10, 20, 40, 80 and 120 mAcm^{-2}. Al^{3+} has a strong and fast effect on electrochemical properties of nickel hydroxide.[59,68] Thereby, GCD during 10 cycles per each current density was enough for Al^{3+} impact estimation. Specific capacities C_{spec} (Fg^{-1}) and Q_{spec} (mAhg^{-1}) have been calculated based on CDC results. Specific capacities have been calculated taking into account the loading of nickel hydroxide samples in the working electrode.

Results and Discussion

Aluminum content of samples and discussion on the possible mechanism of its incorporation.—During the direct synthesis of nickel hydroxide with aluminum additive,[29,30,33–35] Al^{3+} is incorporated into hydroxide crystal lattice a guest. This results in the formation of monophase LDH, a singular compound with increased electrochemical properties. As such the aluminum plays the role of structural activator. However, the role of aluminum absorbed onto the nickel hydroxide surface is not entirely clear. According to Ezhov,[68] Al^{3+} on the surface of nickel hydroxide decreases the polarization of O_2 evolution. This prevents nickel hydroxide from charging completely, which lowers its specific capacity. During the hot hydrolysis stage of the two-step, high-temperature synthesis[55] nickel hydroxide particle is formed on the nickelate particle surface. The mechanism of this reaction is not clear, but the assumption is this is a ≪Solid-state– Liquid-state≫ mechanism. This mechanism assumes the dissolution of nickel-containing forms and transfer of ions, most likely as absorbed ions, to the location of crystal growth. In this work, high-temperature two-step synthesis of nickel hydroxide with the introduction of aluminum perchlorate to initial solution was attempted. Properties of the final product (nickel hydroxide), including Al^{3+} content, are primarily governed by the state of aluminum in reaction vessel after the first stage (precursor synthesis). This would further affect the process that occurs during the second strange (hydrolysis stage). Synthesis of precursor (sodium nickelate) for sample NiAl 10% was conducted to determine precursor composition and mechanism of aluminum incorporation into final hydroxide. Three possible mechanisms were proposed:

"Solid—Liquid—Solid" mechanism.—Aluminum and nickel cations form precursor precipitate and transform into nickel hydroxide during hydrolysis. There are two possible cases:

(a) "Joint-Solid—Liquid—Solid" mechanism (JS-L-S). Aluminum cations are incorporated into precursor as a result of co-crystallization, forming a single phase with sodium nickelate. In this case, the aluminum content in the precursor should be about the same as it was in the initial solution. The formed phase has a single set of properties and acts as a single compound during hydrolysis. Aluminum is incorporated into nickel hydroxide via a liquid-phase mechanism, but simultaneously with nickel cation. In these cases, the probability for aluminum incorporation into the crystal lattice of forming $Ni(OH)_2$ is the highest. The hydroxide formed this way should be most active due to the activating role of aluminum in structure.

(b) "Separate-Solid—Liquid—Solid" mechanism (SS-L-S). Aluminum forms a separate phase of sodium aluminate in precursor precipitate. In this case, the aluminum could be incorporated during hydrolysis through the liquid-phase mechanism, however, the separate aluminum-containing phase would possess properties different from sodium nickelate. In this case, the aluminum content (% mol.) would be different in different parts of the precipitate. This would mean that partial absorption of the aluminum onto the surface of nickel hydroxide is possible.

"Liquid—Liquid—Solid" mechanism (L-L-S).—During the first synthesis stage, the majority of aluminum would be in basic mother liquid. During hydrolysis would be incorporated into nickel hydroxide as a surface additive.

It should be noted, that under real conditions and different aluminum content, it possible that few mechanisms would realize simultaneously.

To study if the SS-L-S mechanism occurs, structural features of sodium nickelate and sodium aluminate were analyzed. Generally, nickelates and aluminates of sodium have a hexagonal and orthorhombic lattice structure. The attention was mainly focused on nickelates and aluminates with a hexagonal lattice. Nickelates and aluminates with the same space groups were found, but lattice parameters were rather different. Thus it was concluded that there was no isostructural sodium aluminates and nickelates. The most likely scenario is that sodium aluminate is incorporated into precursor precipitate as a separate phase, indicating the realization of SS-L-S mechanism. EDX results for sample NiAl 10% precursor (Fig. 1g) shows significant variability in aluminum content (0% to 9.3%). This indicates the realization of SS-L-S mechanism. Hot and cold hydrolysis samples show a significant difference in aluminum content compared to the initial solution. It should be noted that the difference in ionic radii of Ni^{2+} and Al^{3+} is more than 20%, which indicates that the direct substitution of Ni^{2+} with Al^{3+} in the crystal lattice is impossible, but the formation of interstitial solid solution is possible. However, charge difference possess an obstacle for such solution formation. Substitution of nickel with aluminum is known occurrence in LDH, however there the excessive charge is compensated by anions intercalated into interlayer space. Such α-like (or high defected β_{bc}-structure) is characteristics for samples of cold hydrolysis. Aluminum content in cold hydrolysis samples is significantly higher than that for hot hydrolysis samples. For samples, NiAl 3% cold (Fig. 1f) and NiAl 5% cold (Fig. 1d) aluminum content is close to that in the initial solution. However, for sample NiAl 10% cold (Fig. 1b) aluminum contentment is significantly lower– 4.6%–6.7% compared to 10% that was initially added. It is possible, that 7% (mol.) is the maximum aluminum content for β_{bc}-$Ni(OH)_2$ and α-$Ni(OH)_2$. It should be noted that the difference in ionic radii of Ni^{2+} and Al^{3+} is more than 20%, which indicated that the incorporation of aluminum should be possible only with the formation of the interstitial solid solution with some deformations of the crystal lattice. However, compensation of excessive charge requires the incorporation of additional anions, which is difficult for highly crystalline β-$Ni(OH)_2$. As such doping of highly crystalline β-$Ni(OH)_2$ with small amounts of aluminum should be possible. This conclusion is supported by the results of EDX and chemical analysis (Table II) for samples NiAl 10% hot (Fig. 1a), NiAl 5% hot (Fig. 1c) and NiAl 3% hot (Fig. 1e), for which aluminum content doesn't exceed 1.8% (mol.).

Influences of Al^{3+} additive on crystal structure and morphology of nickel hydroxide particles.—As previously described,[55] both cold and hot hydrolysis result β-$Ni(OH)_2$, but with different crystallinity. It was detected, that the structure of reference samples (Ni Pure Hot and No Pure Cold) corresponds to standard #00–073–1520 $Ni(OH)_2$ (hexagonal crystal system, space group P-3m1, cell parameters a = 3.114 Å, c = 4.617 Å), which is β-$Ni(OH)_2$. For comparison α-$Ni(OH)_2$ standard #00–022–0444 $3Ni(OH)_2\cdot2H_2O$ (hexagonal crystal system, space group P-31m, cell parameters a = 5.34 Å, c = 7.5 Å) was used. The principal difference between β-$Ni(OH)_2$ (#00–073–1520 $Ni(OH)_2$) and α-$Ni(OH)_2$ (#00–022–0444 $3Ni(OH)_2\cdot2H_2O$), which have similar crystal hexagonal structure, is cell parameter "c" − 4.617 Å, plate (001) and 7.5 Å, plate (100) respectively. For Co Kα radiation, peaks for these plates are situated at $2\Theta = 22.4°$ for β-$Ni(OH)_2$ and $2\Theta = 13.5°$ for α-$Ni(OH)_2$. Ni Pure Cold sample has a more defective structure, which in literature is referred to as β_{bc}-$Ni(OH)_2$.[22,23] Based on PXRD results (Fig. 2a), it was found that the addition of aluminum results in sample crystallinity sharp decreasing in series NiAl 3% cold—NiAl 5% cold—NiAl 10% cold. Sample NiAl 10% cold is practically X-ray amorphous. The same tendency is observed for hot hydrolysis samples (Fig. 2b). All hot hydrolysis samples (Al-added and Pure), have the characteristic clear peak of β-$Ni(OH)_2$ at $2\Theta = 22.2°–22.5°$. But in the diffractogram of samples with Al-addition, a poorly defined, extra-wide peak of another phase at $2\Theta = 16.1°–18.3°$ was detected. It was suggested that the detected phase is a nickel hydroxide hexagonal phase, which is intermediate between β-$Ni(OH)_2$ ($2\Theta = 22.4°$) and α-$Ni(OH)_2$ ($2\Theta = 13.5°$). Based on a suggestion, the value of parameter "c" has been estimated in

Table I. Potentials and specific currents of anodic and cathodic peaks for nickel hydroxide samples with different Al^{3+} content.

Sample	Real Al^{3+} content (% mol)	Anodic (charge) curve				Cathodic (discharge) curve	
		1st peak		2nd peak		I_{spec}, Ag^{-1}, I_{spec}, Ag^{-1},	Ec, mV Ea, mV
		I_{spec}, Ag^{-1},		Ea, mV			
NiAl 10% hot	0.38–1.83	0.59	495	1.5	603	1.72	439
NiAl 10% cold	4.69–6.40	—	—	3.72	590	3.44	426
NiAl 5% hot	0.76–1.66	3.03	496	1.75	583	3.00	434
NiAl 5% cold	3.93–5.05	1.99	492	5.23	569	4.65	438
NiAl 3% hot	0.92–1.04	3.53	489	3.41	569	5.77	429
NiAl 3% cold	2.04–3.18	2.44	500	5.77	634	4.85	430

5.6–6.3 Å. It should be noted that β-Ni(OH)$_2$ is anhydrous Ni(OH)$_2$, α-Ni(OH)$_2$ is 3Ni(OH)$_2$·2H$_2$O, crystalline hydrate. Therefore, this phase also is α-like Ni(OH)$_2$ with less amount of water, than in α-Ni(OH)$_2$. Increasing of aluminum content leads to increasing of the amounts of this α-like Ni(OH)$_2$ phase. The evidence of this is the increasing of intensity of the extra-wide peak. At the same time, crystallinity of this phase in the all samples is low. Peaks of main, β-Ni(OH)$_2$ phase, get broader and their intensity decreases. This indicates the presence of some amount of the alpha-phase domains or stacking faults.[69] Calculation of cell parameters and crystallinity was not successful by the reason for an extra high level of sample texturing. An increase in a number of structural defects is further supported by SEM and TEM images. For samples NiAl 3% hot (Figs. 3a, 3b) and NiAl 3% cold (Figs. 3e, 3f), particle morphology doesn't differ significantly from that of nickel hydroxide prepared by two-step high-temperature synthesis at cold or hot hydrolysis without aluminum additive.[55] Sample NiAl 3% hot has ≪pseudo-single≫ particles, composed of hexagonal primal nanoparticles with a thickness of 30–40 nm. Sample NiAl 3% cold is composed of larger hexagonal particles stacked together. It is possible, that the addition of 3% Al results in doping of nickel hydroxide with the incorporation of aluminum into the crystal lattice, without significant changes in particle morphology. Increasing aluminum content to 10% leads to particle deformation for both cold and hot hydrolysis. Hot hydrolysis sample NiAl 10% hot is also composed of ≪pseudo-single≫ particles, however, the hexagonal shape of primal particles is strongly deformed (Fig. 4c). TEM images (Fig. 4d) show that primal particles are coated with layers with a total thickness of 15–20 nm, which appears to be a core–shell structure. It is likely, that surface layer is defective, amorphous β_{bc}-Ni(OH)$_2$ (which is seen as X-ray amorphous component on PXRD patterns), that contains aluminum cations. Cold hydrolysis sample NiAl 10% cold (Fig. 4g) is composed of spherical particles 80–190 nm in diameters. During cold hydrolysis, the aluminum cations are absorbed onto the surface of forming the hydroxide, altering particle growth rate in different directions, which results in spherical particles.

Results of DTG and DSC analyses support PXRD data. TG curves of NiAl 10% hot (Fig. 4a), NiAl 5% hot (Fig. 4b) and NiAl 3% hot (Fig. 4c), are characterized the hot hydrolysis samples as a high crystalline β-Ni(OH)$_2$.[53,65] In this case, there is only one weight loss step (16%–19.3%) at the temperature around 300 °C, corresponded to nickel hydroxide decomposition with nickel oxide obtaining:

$$Ni(OH)_2 \rightarrow NiO + H_2O \qquad [3]$$
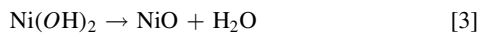
This is confirmed by the DSC curves showing a single endothermic peak at the t = 297 °C–312 °C. The cold hydrolysis sample NiAl 10% cold (Fig. 4d), NiAl 5% cold (Fig. 4e) and NiAl 3% cold (Fig. 4f) exhibit a two-weight loss step TG curve: a first step at the temperature range 60 °C–100 °C range and a second step with weight loss (6.22%) at the temperature 240 °C—340 °C. The first weight loss does not correspond with sharp calorimetric peaks

and can thus be attributed to water, containing in the defect sites which are typical for badly crystallized β-phases.[69] The second weight loss associated with the sharp endothermic peak, related to the hydroxide degradation to NiO. These parameters are similar to thermal characteristics of pure Ni(OH)$_2$, prepared by high-temperature two-step synthesis.[55] The addition of aluminum has no significant effect on the thermal behavior of hot hydrolysis samples. For cold hydrolysis samples, the first endothermic peak is split into few[55] broad peaks. First endothermic peaks characterize the thermal removal of crystalline and defect water and depend on water quantity and bond energy. According to the proposed mechanism, Al^{3+} incorporation occurs in the surface layer. Therefore there are few broad peaks in the first endothermic peak, which correspond to water removal from different deepness layers. According to XRD results, increasing of Al^{3+} additive to cold hydrolysis samples give the decreasing of the samples crystallinity, and as a result—decreasing the water quantity in the crystal lattice defects.

Influence of Al^{3+} additive on electrochemical properties of nickel hydroxide.—The electrochemical activity (mass utility) of nickel hydroxide in the positive electrode of the alkaline Ni-Co, Ni-Fe, Ni-MeH secondary cell is strong determined by specific surface, proton diffusion rate in the particle and overpotentials of two electrochemical reactions under charge process: nickel hydroxide oxidation to oxyhydroxide and oxygen evolution. The two last parameters are based on polymorph type of nickel hydroxide (α, β, or $\alpha + \beta$[25,26,81]) and it crystallinity.[2,3,42]

The electrochemical activity of Ni(OH)$_2$ used in supercapacitors is governed by a number of factors. In[51] is described that main parameters are: (1) type of nickel hydroxide (α, β, or $\alpha + \beta$), which determines own electrochemical activity; (2) crystallinity, which determines the depth of electrochemical process; (3) particle size, specific surface area. Electrochemical properties of pure nickel hydroxide prepared by high-temperature two-step synthesis with cold and hot hydrolysis were studied previously.[55] In general, without additives, the different crystallinity and particle morphology of hot and cold hydrolysis samples give different electrochemical activities. The hot hydrolysis sample has higher cycling stability and reversibility but has decreased capacity. These data based on the increased surface area, probably resulting from the hexagonal "pseudo-single" morphology, but decreased proton diffusion rate, usually observed for high crystallized structures.[55]

Influence of Al^{3+} has been investigated by cyclic voltammetry and galvanostatic charge-discharge cycling.

Cyclic voltammetry at a scan rate of 1 mVs^{-1}, is approximately equal to alkaline secondary cells mode with low charge-discharge rate, revealed that cold hydrolysis samples (NiAl 10% cold—Fig. 5b, NiAl 5% cold—Fig. 5d, NiAl 3% cold—Fig. 5f) have higher peak current in comparison to hot hydrolysis samples (NiAl 10% hot—Fig. 5a, NiAl 5% hot—Fig. 5c, NiAl 3% hot—Fig. 5e). This indicates that cold hydrolysis samples possess higher electrochemical activity than hot hydrolysis samples, which is in agreement
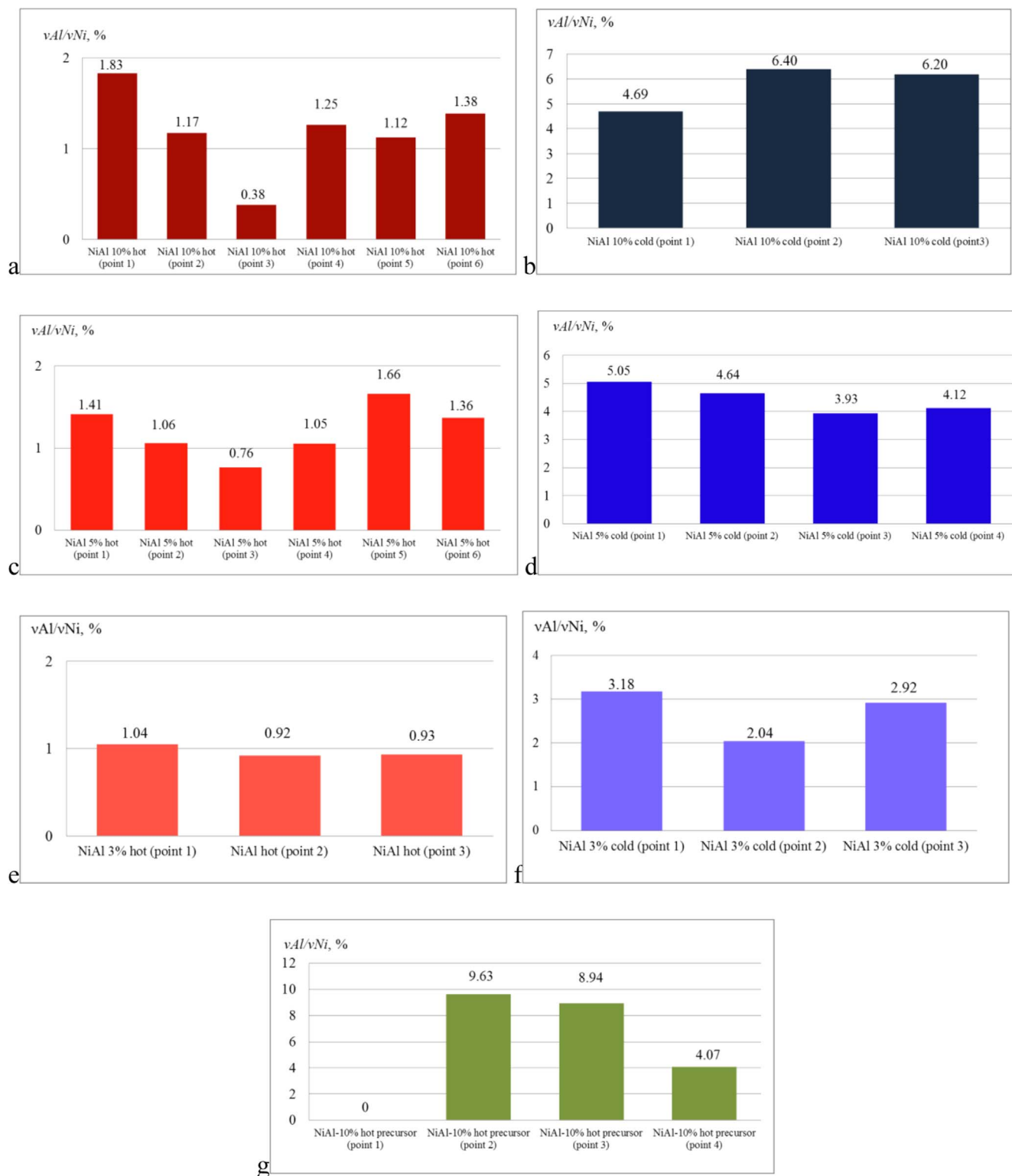
Figure 1. Al:Ni molar ratio (%) of different Ni(OH)$_2$ samples with Al additive (calculated from results of EDX): (a) NiAl 10% hot; (b) NiAl 10% cold; (c) NiAl 5% hot; (d) NiAl 5% cold; (e) NiAl 3% hot; (f) NiAl 3% cold; (g) NiAl 10% precursor.

with data for pure nickel hydroxide prepared by high-temperature solid-state synthesis.[55] Increasing aluminum content in the initial solution from 3% (mol.) to 10% (mol.) has no significant effect on the electrochemical characteristics of samples. It can be noted, that at a low scan rate (in the secondary cell mode) no activating or poisoning effect of aluminum additive is observed.

To study electrochemical behavior at a higher rate of the electrochemical process (supercapacitor mode), the cyclic voltammetry was conducted at different scan rates (1, 2, 5, 10 and 50 mVs^{-1}). Such method is widely used for the characterization of Ni(OH)$_2$, NiO and Ni-LDH specially as an active substance of hybrid supercapacitor.[43,70–75]
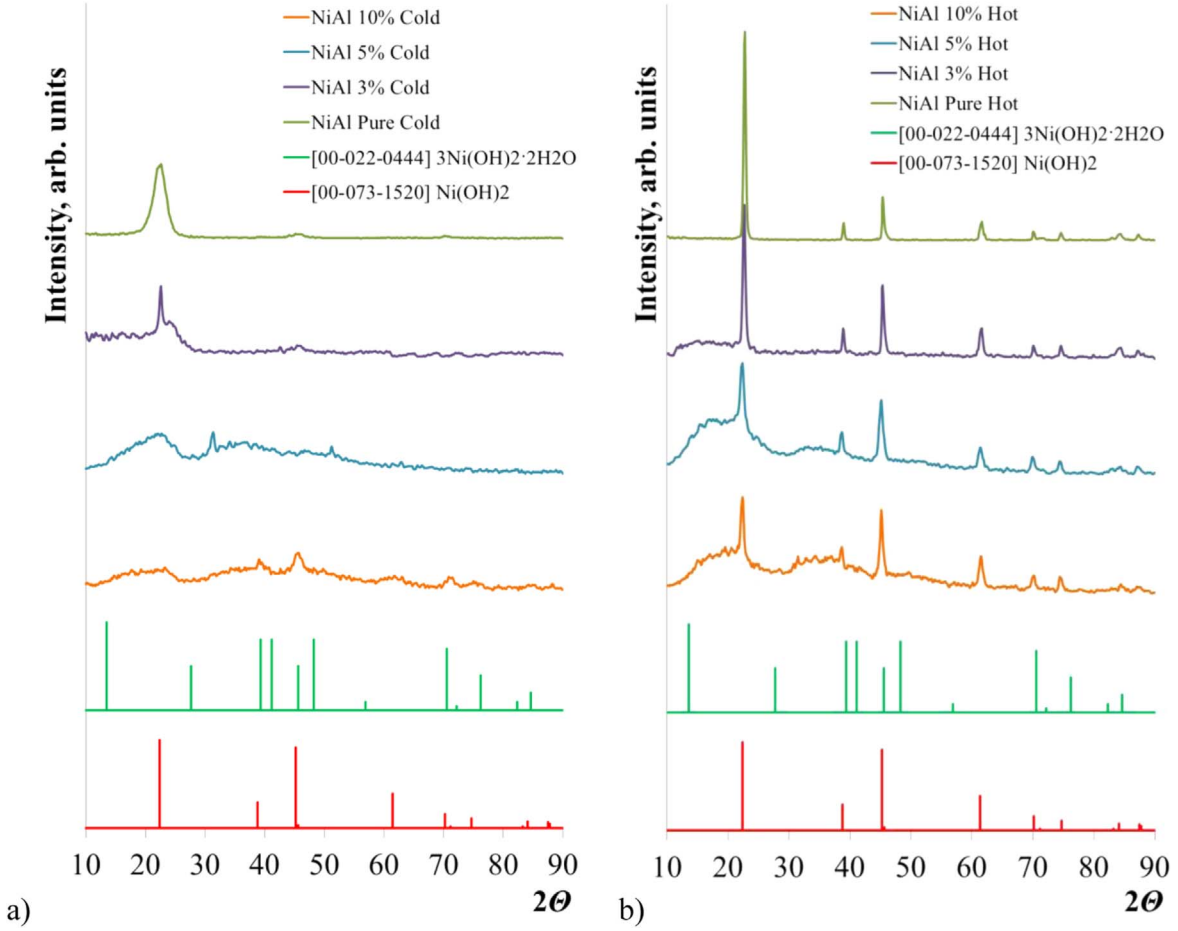
Figure 2. PXRDpatterns of Ni(OH)$_2$ samples with aluminium additive obtained by two-step high-temperature synthesis: (a) cold hydrolysis; (b) hot hydrolysis.

Table II. Comparison of theoretical and experimental νAl: νNi (molar %) for nickel hydroxide samples with different Al^{3+} addition.

Sample	Theoretical	Chemical method	EDX					
NiAl 10% Precursor	10	—	0	9.63	8.94	4.07		
NiAl 10% Hot	10	1.35	1.83	1.17	0.38	1.25	1.12	1.38
NiAl 5% Hot	5	1.12	1.41	1.06	0.76	1.05	1.66	1.36
NiAl 3% Hot	3	0.99	1.04	0.92	0.93	—	—	—
NiAl 10% Cold	10	6.02	4.69	6.40	6.20	—	—	—
NiAl 5% Cold	5	4.70	5.05	4.64	3.93	4.12	—	—
NiAl 3% Cold	3	2.89	3.18	2.04	2.94	—	—	—

CVA curves are shown in Fig. 6. The scan rate of 50 mVs^{-1} corresponds to high rates of charge and discharge of samples. At this scan rates, curves of almost all samples show two charge peaks, one at 490–500 mV, and second at 570–630 mV. In the general case, two charge peaks in the CV curves are characterized by the same reaction:

$$\mathrm{Ni(OH)_2} - 1e^- \rightarrow \mathrm{NiOOH} + \mathrm{H}^+ \qquad [4]$$

But different forms of nickel hydroxide (β-Ni(OH)$_2$, β_{bc}-Ni(OH)$_2$ and α-Ni(OH)$_2$) are characterized by different charge potentials, according to their electrochemical activity. Electrochemical activity and the charge potential decreases among the line "α-Ni(OH)$_2$—β_{bc}-Ni(OH)$_2$—β-Ni(OH)$_2$." Crystallinity increasing gives a similar result.[76–79] The presence of two peaks in CV curves describes the double-phase structure of both samples,

included different types of nickel hydroxide. Cold hydrolysis samples consist of β-Ni(OH)$_2$ and β_{bc}-Ni(OH)$_2$. But during cycling meta-stable β_{bc}-hydroxide transforms into stable β-hydroxide, and specific current of the first peak (corresponding to meta-stable β_{bc}-Ni(OH)$_2$) is decreased, and specific current of the second peak (corresponding to β-Ni(OH)$_2$) is increased. There is an apparent contradiction for the hot hydrolysis sample. According to PXRD results (Fig. 2), the hot hydrolysis sample is high crystalline β-Ni(OH)$_2$, but with the presence of few amounts of X-ray amorphous phase. In the[55] this behavior explained by double-phase of hot hydrolysis sample, which consists of nanosized particles with some amount of larger particles. Nanoparticles are characterized by a high percentage of surface nickel atoms. Therefore nanosized β-Ni(OH)$_2$ particles with high crystallinity have α-like electrochemical properties. At the same time, the X-ray amorphous component, formed under Al^{3+} influencing, also have α-like
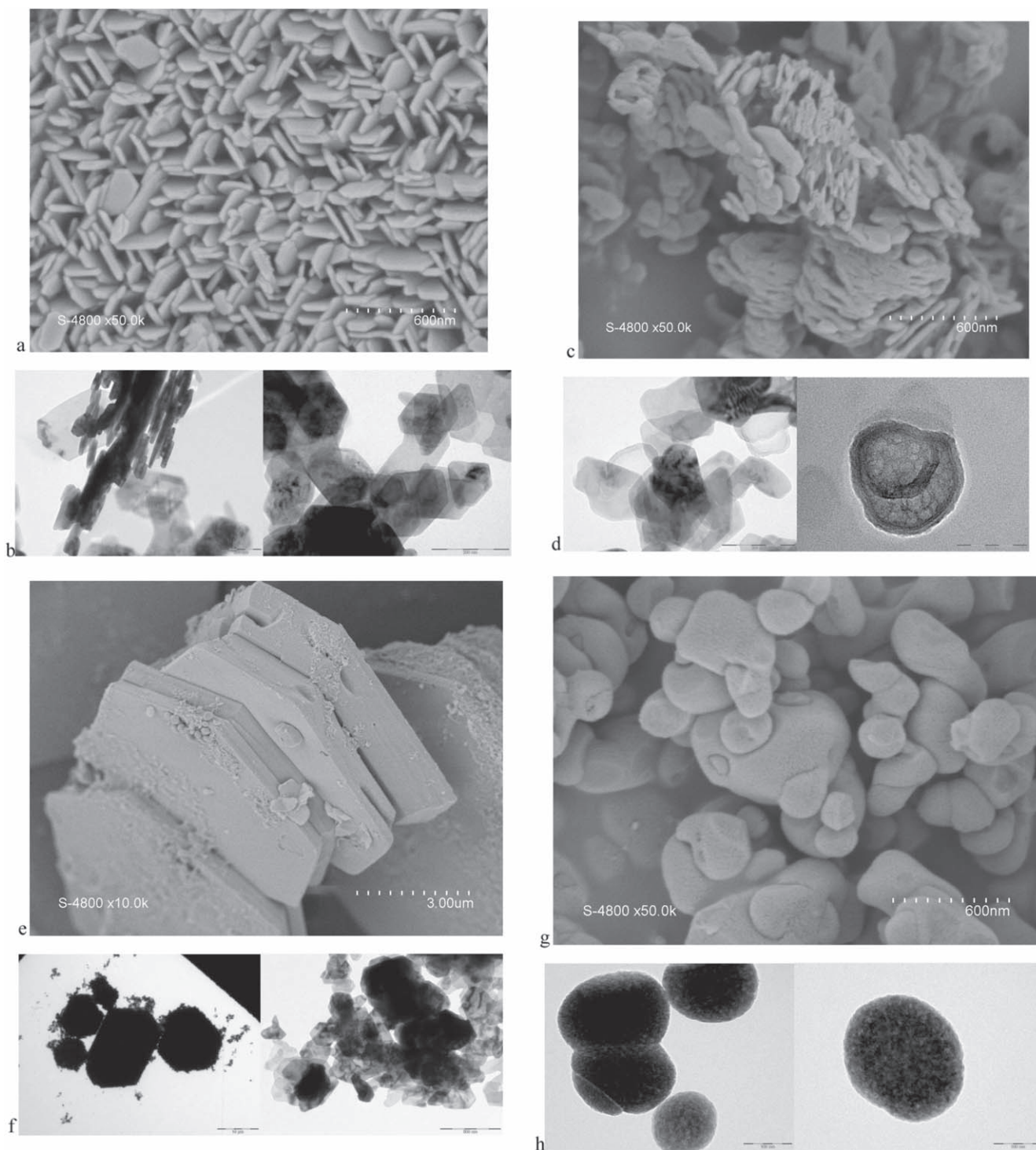
Figure 3. SEM and TEM images of Ni(OH)$_2$ samples with aluminium additive obtained by two-step high-temperature synthesis:(a), (c), (e), (g) SEM images; (b), (d), (f), (h) TEM images; (a), (b) NiAl 3% hot; (c),(d) NiAl 10% hot; (e), (f) NiAl 3% cold; (g), (h) NiAl 10% cold.

electrochemical behavior. As such, the first peak for hot hydrolysis samples (NiAl 3% hot—Fig. 6a; NiAl 5% hot—Fig. 6c; NiAl 10% hot—Fig. 6e) can correspond to nanosized particles of high crystalline β-Ni(OH)$_2$, and X-ray amorphous particles. Analysis of CVA curves at 50 mVs^{-1} for all samples was conducted, lists potentials and specific peak currents are shown in Table I.

Analysis of Table I reveals that for all samples higher Al^{3+} content results in lower specific currents of both charge and discharge peaks. It is worth highlighting the influence of aluminum additive on the first charge peak of cold hydrolysis samples (NiAl

3% cold, NiAl 5% cold and NiAl 10% cold), which characterizes electrochemical activity the most. Decrease of the specific current of first charge peak with an increasing amount of introduced Al^{3+}, and real Al^{3+} content is significant and for sample NiAl 10% cold the first charge peaks disappear. This clearly indicates the poisonous effect of aluminum additive introduced in large amounts. Upon realization of the SS-L-S mechanism, a significant part of the aluminum compound resided on the surface of nickel hydroxide. This supports previous findings of Ezhov,[68] regarding the poisonous effect of surface Al compounds. For hot hydrolysis samples (NiAl
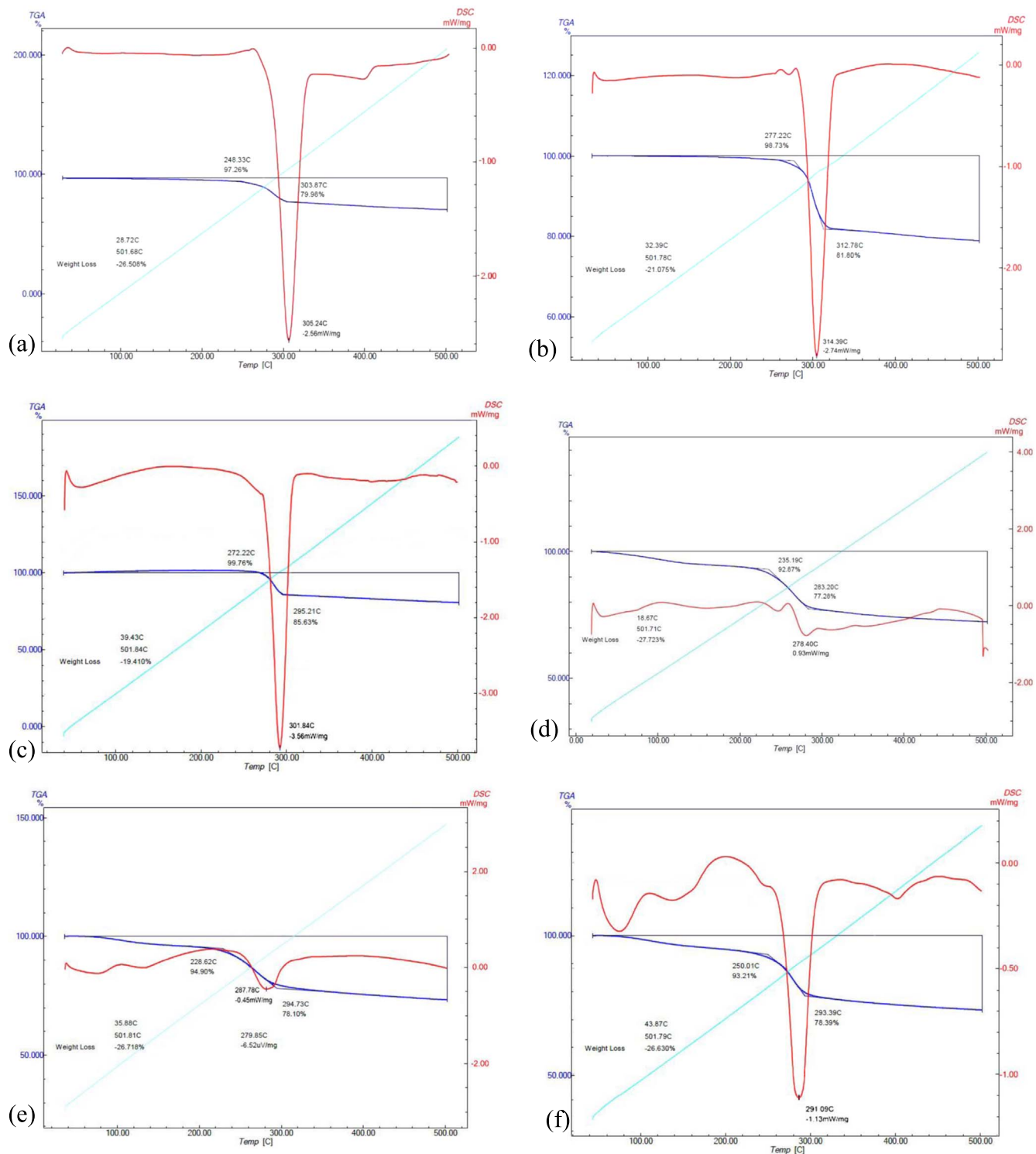
Figure 4. TG and DSC curves of Ni(OH)$_2$ samples with aluminum additive obtained by two-step high-temperature synthesis: (a) NiAl 3% hot; (b) NiAl 5% hot; (c) NiAl 10% hot; (d) NiAl 3% cold; (e) NiAl 5% cold; (f) NiAl 10% cold.

3% hot, NiAl 5% hot and NiAl 10% hot) decrease in specific peak currents is also observed, but to a lesser degree. An interesting fact was discovered. As in previous study,[55] results of the present study (Table I) also show that electrochemical activity during discharge (expressed as the specific peak of discharge) of cold hydrolysis samples is higher than that of hot hydrolysis samples. This is explained by the lower crystallinity of β-Ni(OH)$_2$ and the presence of significant amounts of β_{bc}-Ni(OH)$_2$. However, it was found that

under scan rate of 50 mV c^{-1} (Table I) sample NiAl 3% hot has a specific peak current of 5.77 Ag^{-1}, which is 19% higher than this value of NiAl 3% cold (4.85 Ag^{-1}). This reveals the activating of the effect of small amounts of Al^{3+}. This indicated that under these conditions Al^{3+} is incorporated into the structure of surface layers of nickel hydroxide, and possibly partially replacing Ni^{2+} in the crystal lattice of hydroxide. In this case, aluminum cations play the role of structural activator.[4,5,30,33,34] This can be indicative of partial
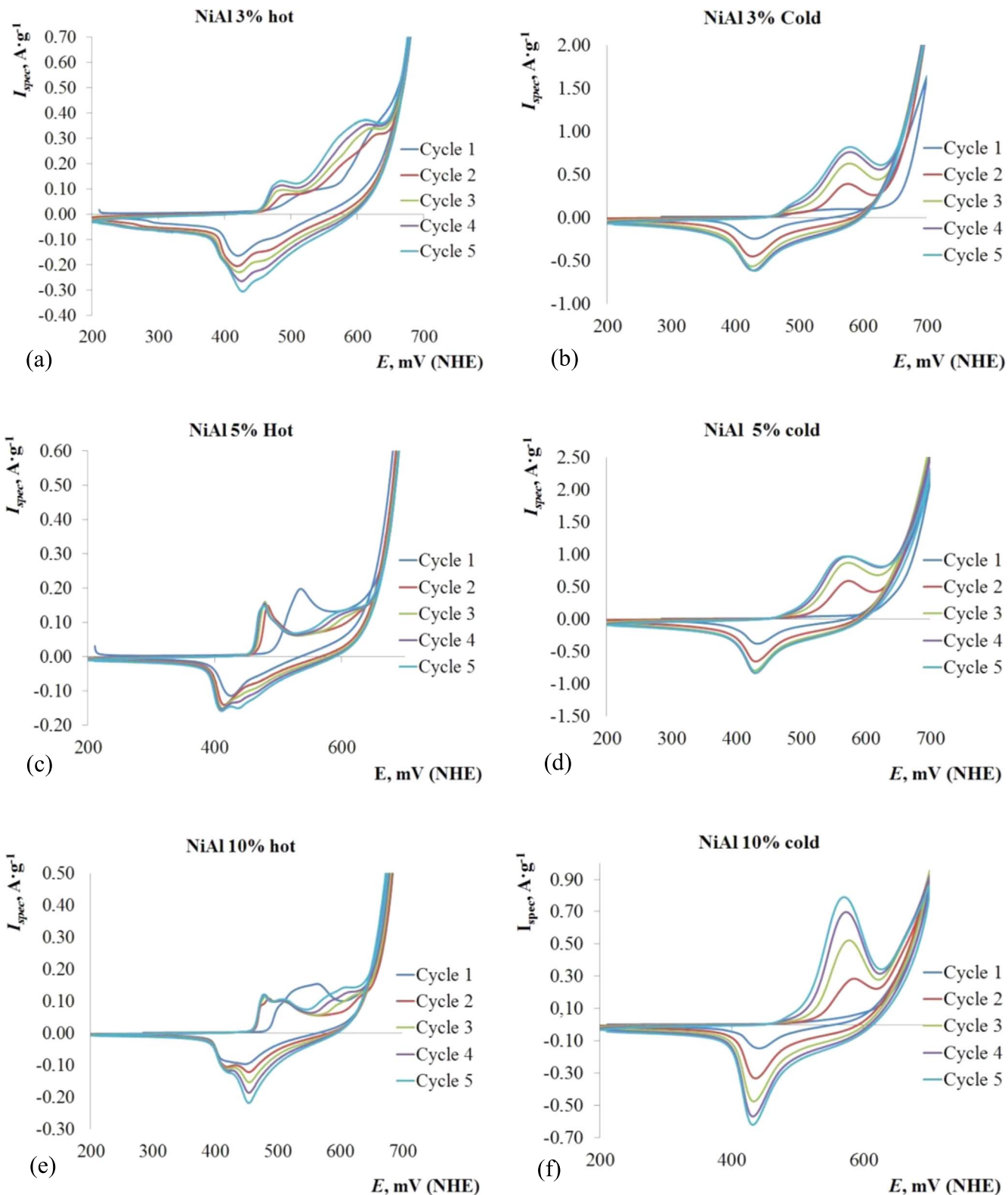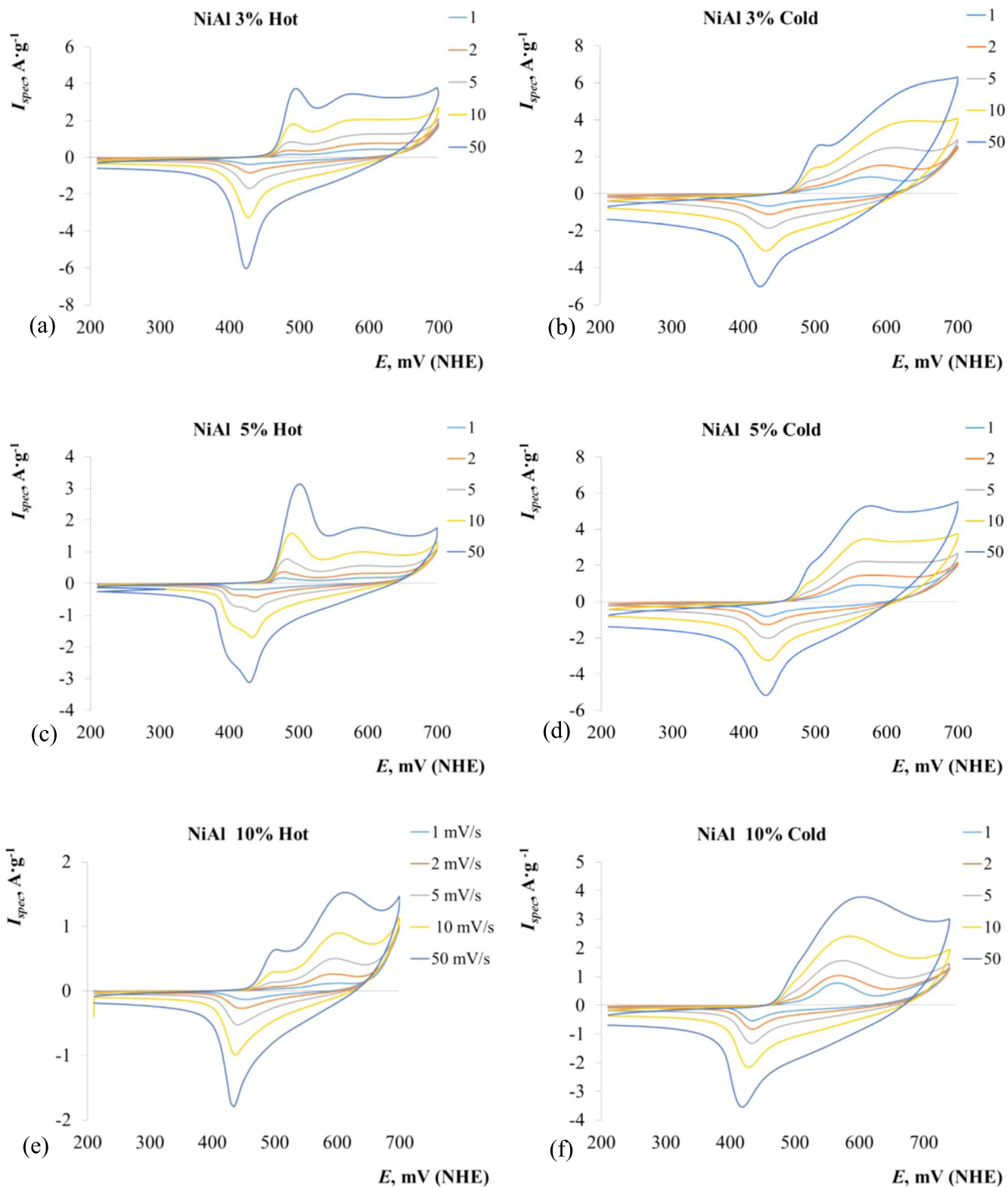
Figure 5. Cyclic voltammograms (scan rate 1 mVs⁻¹) of Ni(OH)$_2$ samples with aluminium addition obtained by two-step high-temperature synthesis: (a) NiAl 3% hot; (b) NiAl 3% cold; (c) NiAl 5% hot; (d) NiAl 5% cold; (e) NiAl 10% hot; (f) NiAl 10% cold.

realization of the JS-L-S mechanism, which at high temperatures allows for crystal lattice of β-Ni(OH)$_2$ to be doped with Al^{3+}.

Data of galvanostatic charge-discharge cycling (Figs. 7a–7d) supports conclusions drawn from cyclic voltammetry results. For comparison, Figs. 7a–7d show specific capacities of pure nickel hydroxides prepared by hot and (Ni pure hot) and cold (Ni pure cold)

hydrolysis (data are taken from Ref. 55). Comparative analysis revealed a significant change in the ratio of specific characteristics of samples of cold and hot hydrolysis for samples with the addition of aluminum and pure nickel hydroxide. For all aluminum contents, specific capacities (Fg⁻¹ and mAhg⁻¹) for hot hydrolysis samples are higher than those of cold hydrolysis samples. This clearly shows

Figure 6. Cyclicvoltammograms (scan rate 1–50 mVs^{-1}) of Ni(OH)$_2$ samples with aluminium addition obtained by two-step high-temperature synthesis: (a) NiAl 3% hot; (b) NiAl 3% cold; (c) NiAl 5% hot; (d) NiAl 5% cold; (e) NiAl 10% hot; (f) NiAl 10% cold (line captures—scan rate, mVs^{-1}).

the poisonous effect of Al^{3+} compounds on nickel hydroxide of cold hydrolysis. Addition of 3% (mol.) Al^{3+} for cold hydrolysis decreases specific capacity by 3.86 times (from 1057 Fg^{-1} Ni pure cold to 275 Fg^{-1} NiAl 3% cold). Further increase of added Al^{3+}, results in a higher content of aluminum in the sample, which further decreases specific capacity. However, it should be detected, that the effect of

Al^{3+} on Ni(OH)$_2$ prepared by cold hydrolysis is not limited by poisoning. Increasing cycling current dense in series «10–20–40––80–120 mAcm^{-2}» does not result in lower capacity, but results in some capacity aging «275–274–280–291–323 Fg^{-1}». This indicates the known stabilizing effect of Al^{3+} on α-Ni(OH)$_2$.[56–59,64,80] It can be concluded, that Al^{3+} also has a stabilizing effect on
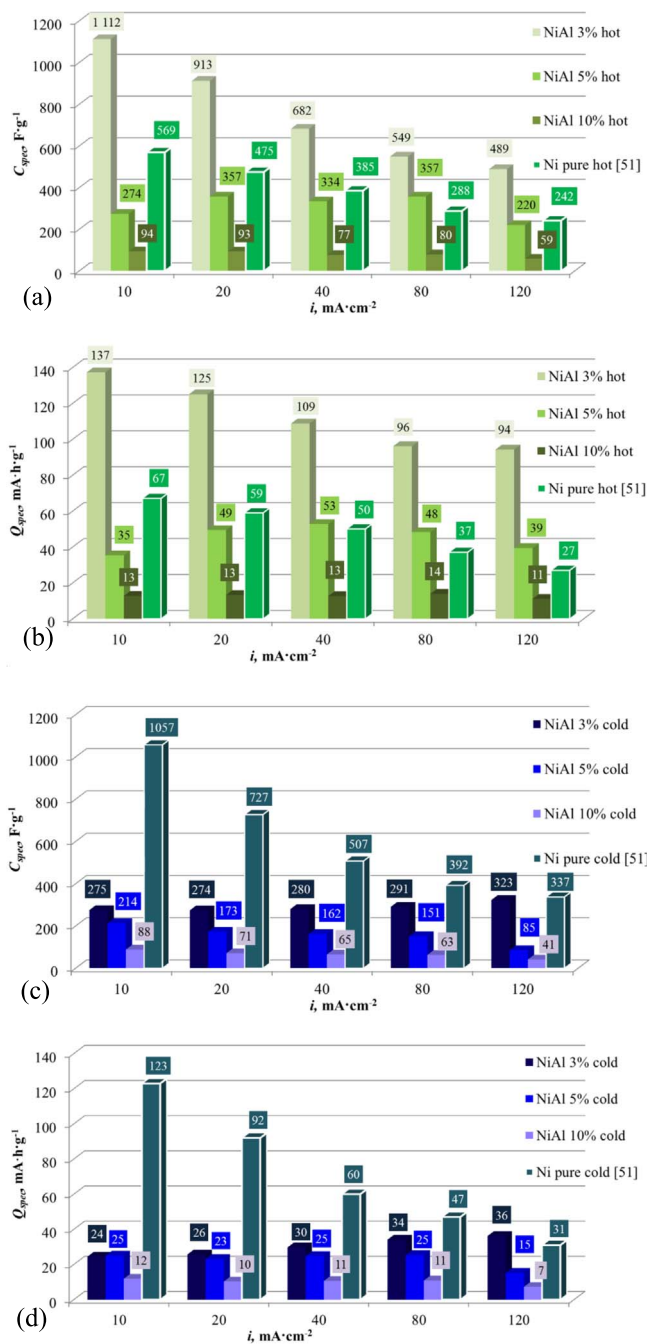
Figure 7. Specific characteristics of Ni(OH)$_2$ samples with aluminum additive obtained by two-step high-temperature synthesis with (a), (b) hot hydrolysis; (c), (d) cold hydrolysis, calculated from galvanostatic CDC: (a), (c) C_{spec}^{full}, Fg^{-1}; (b), (d) Q_{spec}^{full}, mAhg^{-1}.

β_{bc}-Ni(OH)$_2$, which primarily responsible for the electrochemical activity of cold hydrolysis samples, similar to what's been described in Ref. 66. The stabilizing effect comes from aluminum cations that were incorporated into the crystal lattice of nickel hydroxide. As such it can be concluded, that during cold hydrolysis part of aluminum cations is incorporated into hydroxide lattice. However, a further increase of aluminum content in the synthesis solution (and real content), the poisonous effect of aluminum outweighs its stabilizing effect. For hot hydrolysis samples, the increase of aluminum content also results in a capacity loss, but to a lesser degree. Additionally, despite increasing aluminum content in the synthesis solution, the final content in resulted samples was roughly the same. It is possible, that redistribution between Al^{3+} present in

the crystal lattice and Al^{3+} on the surface occurs. This results in an increase of surface aluminum. This is supported by specific characteristics of sample NiAl 3% hot, the specific capacity of which (1112 Fg^{-1}) exceeds the capacity of reference sample Ni pure hot (pure nickel hydroxide hot hydrolysis[55]) by 1.95 times and sample NiAl 3% cold by 4.04 time. This indicates the significant activating effect of small amounts of aluminum. Increasing cycling current density leads to lower specific capacity and less pronounced activating effect.

Conclusions

(1) Influence of Al^{3+} additive on characteristics of nickel hydroxide prepared by two-step high-temperature synthesis with the use of hot (170 °C, 24 h) and cold (20 °C, 24 h) hydrolysis has been studied. A series of Ni(OH)$_2$ samples have been prepared with the addition of aluminum perchlorate to the solution of initial compounds (nickel perchlorate) in ratios 3%, 5% and 10% (mol.) Al^{3+} to Ni^{2+}. Physical, structural and electrochemical properties of obtained samples have been investigated. A precursor sample—sodium nickelate with the introduction of the maximum amount of Al^{3+} (10% mol.) by stopping the synthesis procedure after the first stage has been synthesized.

(2) It was proposed the mechanism, that describes the formation of nickel hydroxide during two-step high-temperature synthesis with Al^{3+} additive to initial solution, which we call "Separate-Solid—Liquid—Solid." On the first stage, aluminum forms a separate phase of sodium or nickel aluminates. During hydrolysis aluminum through liquid phase mechanism can be incorporated into forming hydroxide powder in two ways:

    (a) by incorporating into the structure;
    (b) by forming aluminum compounds on the surface of particles.

The realization of the proposed mechanism on the first stage is confirmed by theoretical analysis of nickelates and aluminates of sodium, which revealed the absence of isostructural forms, and significant variance in aluminum content in a different part of precursor, determined by EDX. The study of hydroxide samples by means of PXRD, SEM, TEM, and EDX revealed the realization of both ways of aluminum incorporation.

PXRD revealed that the addition of Al^{3+} results in lower crystallinity of samples prepared by cold hydrolysis. For hot hydrolysis samples, the introduction of Al^{3+} in crystal lattice decreases of highly-crystalline component (β-Ni(OH)$_2$) and form of X-ray amorphous component, which is highly defective β_{bc}-Ni(OH)$_2$.

By means of SEM and TEM it was found that at low amounts of Al^{3+} (3% mol.) morphology and particle size don't differ much from pure nickel hydroxide: hot hydrolysis results in the formation of nanostructured «pseudo-single» particles, and cold hydrolysis-large hexagonal submicron particles stacked together. This indicated the doping of Ni(OH)$_2$ by the aluminum cation. An increasing amount of added Al^{3+} to 10% (mol.) results in the significant defection of primal nanosized particles of hot hydrolysis sample; for cold hydrolysis, this results in the formation of spherical particles. This indicated the formation of a surface layer of Al^{3+} compounds, which is supported by the appearance of "core–shell" type particles on TEM images.

By means of EDX analysis, it was found that aluminum content in hot hydrolysis samples is significantly lower in comparison to cold hydrolysis samples. It was also found that hot hydrolysis samples contained significantly less Al^{3+} than what was in the initial solution. Upon introduction of 3% (mol.) Al^{3+} to an initial solution, the aluminum content in nickel hydroxide was 0.792–1.04% (mol.).

(1) By means of cycling voltammetry at the low scan rate of 1 mVs^{-1}, the influence of Al^{3+} additive on electrochemical properties of samples as a secondary cell active substance has

been investigated. No activating or poisoning effect of aluminum additive is detected.

(1) By means of cycling voltammetry and galvanostatic charge-discharge cycling at different current densities, the influence of Al^{3+} additive on electrochemical properties of samples has been investigated. It was found that Al^{3+} can acts as a poison, activator or stabilizer. Under conditions for the formation of aluminum compounds (cold hydrolysis samples and high amounts of introduced Al^{3+} for both hydrolysis types) electrochemical activity and specific characteristics of samples decrease significantly as a result of poisoning. It was found that when doped with aluminum cation, Al^{3+} plays the role of activator and stabilizer of activity. Addition of 3% (mol) Al^{3+} leads to improved capacity of hot hydrolysis sample by 1.95, in comparison to pure nickel hydroxide reference sample (1112 Fg^{-1} and 569 Fg^{-1} respectively). Also, upon addition of 3% (mol.), the stabilizing effect of Al^{3+} was discovered, which manifested in stable (and even increasing) specific capacity of about 275–323 Fg^{-1} with an increase of cycling current density from 10 mA·cm^{-2} to 120 mA cm^{-2}.

ORCID

V. L. Kovalenko   https://orcid.org/0000-0002-8012-6732

References

1. D. S. Hall, D. J. Lockwood, C. Bock, and B. R. MacDougall, *Proc. R. Soc. A*, **471**, 20140792 (2014).
2. M. Vidotti, R. Torresi, and S. I. C. de Torresi, *Quim. Nova*, **33**, 2176 (2010).
3. J. Chen, *J. Electrochem. Soc.*, **146**, 3606 (1999).
4. H. Chen, J. M. Wang, T. Pan, Y. L. Zhao, J. Q. Zhang, and C. N. Cao, *J. Power Sources*, **143**, 243 (2005).
5. P. V. Kamath, M. Dixit, L. Indira, A. K. Shukla, V. G. Kumar, and N. Munichandraiah, *J. Electrochem. Soc.*, **141**, 2956 (1994).
6. V. Kovalenko and V. Kotok, *East.-Eur. J. Enterp. Technol.*, **3**, 32 (2018).
7. V. Kovalenko and V. Kotok, *East.-Eur. J. Enterp. Technol.*, **4**, 17 (2017).
8. P. E. Lokhande and U. S. Chavan, *Materials Science for Energy Technologies*, **2**, 52 (2019).
9. J.-W. Lang, L.-B. Kong, W.-J. Wu, M. Liu, Y.-C. Luo, and L. Kang, *J. Solid State Electrochem.*, **13**, 333 (2009).
10. S. Min, C. Zhao, G. Chen, and X. Qian, *Elec. Acta*, **115**, 155 (2014).
11. J.-W. Lang, L.-B. Kong, M. Liu, Y.-C. Luo, and L. Kang, *J. Solid State Electrochem.*, **14**, 1533 (2010).
12. M. Aghazadeh, M. Ghaemi, B. Sabour, and S. Dalvand, *J. Solid State Electrochem.*, **18**, 1569 (2014).
13. C.-H. Zheng, X. Liu, Z.-D. Chen, Z.-F. Wu, and D.-L. Fang, *J. Cent. South Univ.*, **21**, 2596 (2014).
14. B. Wang, W. R. Gareth, Z. Chang, M. Jiang, J. Liu, X. Lei, and X. Sun, *ACS Appl. Mater. Interfaces*, **6**, 16304 (2014).
15. V. Kotok and V. Kovalenko, *East.-Eur. J. Enterp. Technol.*, **4**, 31 (2017).
16. V. A. Kotok, V. L. Kovalenko, V. A. Solovov, P. V. Kovalenko, and B. A. Ananchenko, *ARPN J. Eng. Appl. Sci.*, **13**(9), 3076 (2018).
17. V. Kotok and V. Kovalenko, *East.-Eur. J. Enterp. Technol.*, **5**, 18 (2018).
18. V. A. Kotok, V. V. Malyshev, V. A. Solovov, and V. L. Kovalenko, *ECS J. Solid State Sci. Technol.*, **6**, P772 (2017).
19. V. A. Kotok and V. L. Kovalenko, *J. Electrochem. Soc.*, **166**, D395 (2019).
20. A. Mignani, B. Ballarin, M. Giorgetti, E. Scavetta, D. Tonelli, E. Boanini, V. Prevot, C. Mousty, and A. Iadecola, *J. Phys. Chem. C*, **117**, 16221 (2013).
21. V. Solovov, V. Kovalenko, N. Nikolenko, V. Kotok, and E. Vlasova, *East.-Eur. J. Enterp. Technol.*, **1**, 16 (2017).
22. Y. Fan, Z. Yang, X. Cao, P. Liu, S. Chen, and Z. Cao, *J. Electrochem. Soc.*, **161**, B201 (2014).
23. T. N. Ramesh and P. V. Kamath, *J. of Power Sources*, **156**, 655 (2006).
24. V. Kovalenko and V. Kotok, *East.-Eur. J. Enterp.Technol*, **2**, 16 (2018).
25. V. Kovalenko and V. Kotok, "Influence of the carbonate ion on characteristics of electrochemically synthesized layered $(\alpha+\beta)$ nickel hydroxide." *East.-Eur. J. Enterp. Technol*, **1**, 40 (2019).
26. V. Kovalenko and V. Kotok, *East.-Eur. J. Enterp. Technol*, **3**, 44 (2019).
27. R. S. Jayashree and P. Vishnu Kamath, *J. Appl. Electrochem.*, **31**, 1315 (2001).
28. M. Hu, Z. Yang, L. Lei, and Y. Sun, *J. Power Sources*, **196**, 1569 (2011).
29. S. I. Cordoba de Torresi, K. Provazi, M. Malta, and R. M. Torresi, *J. Electrochem. Soc.*, **148**, A1179 (2001).
30. P. Nalawade, B. Aware, V. J. Kadam, and R. S. Hirlekar, *J. Sci. Ind. Res.*, **68**, 267 (2009).
31. C. Tessier, C. Faure, L. Guerlou-Demourgues, C. Denage, G. Nabias, and C. Delmas, *J. Electrochem. Soc.*, **149**, A1136 (2002).
32. L. Guerlou-Demourgues and C. Delmas, *J. Electrochem. Soc.*, **143**, 561 (1996).
33. B. Liu, X. Y. Wang, H. T. Yuan, Y. S. Zhang, D. Y. Song, and Z. X. Zhou, *J. Appl. Electrochem.*, **29**, 853 (1999).
34. L. Lei, M. Hu, X. Gao, and Y. Sun, *Elec. Acta*, **54**, 671 (2008).
35. Y. W. Li et al., *Int. J. Hydrogen Energy*, **35**, 2539 (2010).
36. V. Kotok, V. Kovalenko, and S. Vlasov, *East.-Eur. J. Enterp. Technol.*, **3**, 6 (2018).
37. V. Kovalenko and V. Kotok, *East.-Eur. J. Enterp. Technol.*, **2**, 11 (2017).
38. L.-X. Yang, Y.-J. Zhu, H. Tong, and Z.-H. Liang, *J. Solid State Chem.*, **180**, 2095 (2007).
39. L. Xu, Y.-S. Ding, C.-H. Chen, L. Zhao, C. Rimkus, R. Joesten, and S. L. Suib, *Chem. Mater.*, **20**, 308 (2008).
40. L. Changjiu and L. Yanwei, *J. Alloys Compd*, **478**, 415 (2009).
41. M. Bora, *Retrospective Theses and Dissertations*, Iowa State University Capstones, Ames, Iowa, USA, 731 (2003).
42. V. Kovalenko and V. Kotok, *East.-Eur. J. Enterp. Technol.*, **5**, 17 (2017).
43. J. Li, F. Luo, X. Tian, Y. Lei, H. Yuan, and D. Xiao, *J. Power Sources*, **243**, 721 (2013).
44. H. Wang, L. Zhang, L. Liu, and S. Park, *J. Electrochem. Soc.*, **166**, D595 (2019).
45. H. Li, F. Musharavati, J. Sun, F. Jaber, E. Zalnezhad, K. N. Hui, and K. S. Hui, *J. Electrochem. Soc.*, **165**, A407 (2018).
46. Y. Zhao, Z. Zhu, and Q.-K. Zhuang, *J. Solid State Electrochem.*, **10**, 914 (2006).
47. Q. Song, Z. Tang, H. Guo, and S. L. I. Chan, *J. Power Sources*, **112**, 428 (2002).
48. P. Oliva, J. Leonardi, J. F. Laurent, C. Delmas, J. J. Braconnier, M. Figlarz, F. Fievet et, and A. de Guibert, *J. Power Sources*, **8**, 229 (1982).
49. P. Simon and Y. Gogotsi, *Nat. Mater.*, **7**, 845 (2008).
50. A. Burke, *Elec. Acta*, **53**, 1083 (2007).
51. V. Kovalenko, V. Kotok, and A. Bolotin, *East.-Eur. J. Enterp. Technol.*, **5**, 17 (2016).
52. C. Tessier, P. H. Haumesser, P. Bernard, and C. Delmas, *J. Electrochem. Soc.*, **146**, 2059 (1999).
53. Q. Li, H. Ni, Y. Cai, X. Cai, Y. Liu, G. Chen, L.-Z. Fan, and Y. Wang, *Mater. Res. Bull.*, **48**, 3518 (2013).
54. G. Sakai, M. Miyazaki, and T. Kijima, *J. Electrochem. Soc.*, **157**, A932 (2010).
55. V. L. Kovalenko et al., *J. Solid State Electrochem.*, **21**, 683 (2017).
56. J. Qi, P. Xu, Z. Lv, X. Liu, and A. J. Wen, *Alloys Compd.*, **462**, 164 (2008).
57. H. Li, Z. Chen, Y. Wang, J. Zhang, and X. Yan, *Elec. Acta*, **210**, 15 (2016).
58. J. Bao, Y. Zhu, Q. S. Xu, Y. H. Zhuang, R. D. Zhao, Y. Y. Zeng, and H. L. Zhong, *Adv. Mater. Res.*, **479**, 230 (2012).
59. M. Hu, X. Gao, L. Lei, and Y. Sun, *J. Phys. Chem. C*, **113**, 7448 (2009).
60. J. Memon et al., *J. Mater. Chem. A.*, **2**, 5060 (2014).
61. C. Y. Wang, S. Zhong, D. H. Bradhurst, H. K. Liu, and S. X. Dou, *J. Alloys Compd.*, **330–332**, 802 (2002).
62. X. Chen, C. Long, C. Lin, T. Wei, J. Yan, L. Jiang, and Z. Fan, *Elec. Acta*, **137**, 352 (2014).
63. M. Hu, X. Ji, L. Lei, and X. Lu, *J. Alloys Compd.*, **578**, 17 (2013).
64. P. Vialat, F. Leroux, and C. Mousty, *J. Solid State Electrochem.*, **19**, 1975 (2015).
65. L. Gourrier, S. Deabate, T. Michel, M. Paillet, P. Hermet, J.-L. Bantignies, and F. Henn, *J. Phys. Chem. C*, **115**, 15007 (2011).
66. V. Kotok and V. Kovalenko, *East.-Eur. J. Enterp. Technol.*, **1**, 4 (2017).
67. Y. Wang, S. Dong, X. Wu, and M. Li, *J. Electrochem. Soc.*, **164**, H56 (2017).
68. B. B. Ezhov and O. G. Malandin, *J. Electrochem. Soc.*, **138**, 885 (1991).
69. M. Rajamathi, P. Vishnu Kamath, and R. Seshadri, *J. Mater. Chem.*, **10**, 503 (2000).
70. H. Li, F. Musharavati, J. Sun, F. J. Aber, E. Zalnezhad, K. N. Hui, and K. S. Hui, *J. Electrochem. Soc.*, **165**, A407 (2018).
71. Y. Fu, J. Song, Y. Zhu, and C. Cao, *J. Power Sources*, **262**, 344 (2014).
72. H. M. Shiria and M. Aghazadeh, *J. Electrochem. Soc.*, **159**, E132 (2012).
73. P. E. Lokhande, K. Pawar, and U. S. Chavan, *Materials Science for Energy Technologies*, **1**, 166 (2018).
74. P. E. Lokhande, U. S. Chavan, and A. Pandey, *Electrochem. Energ. Rev.*, **3**, 1 (2019).
75. W. Ge, W. Peng, A. Encinas, M. Fernanda Ruiz, and S. Song, *Chem. Phys.*, **521**, 55 (2019).
76. T. N. Ramesh, P. V. Kamath, and C. Shivakumara, *J. Electrochem. Soc.*, **152**, A806 (2005).
77. R. S. Jayashree, P. V. Kamath, and G. N. Subbanna, *J. Electrochem. Soc.*, **147**, 2029 (2000).
78. R. S. Jayashree and P. V. Kamath, *J. Electrochem. Soc.*, **149**, A761 (2002).
79. M. N. Tripathi, U. V. Waghmare, T. N. Ramesh, and P. V. Kamath, *J. Electrochem. Soc.*, **157**, A280 (2010).
80. A. Sugimoto, S. Ishida, and K. Hanawa, *J. Electrochem. Soc.*, **146**, 1251 (1999).
81. J. Huang, T. Lei, and X. Wei et al., *J. Power Sources*, **232**, 370 (2013).
82. V. Kovalenko, V. Kotok, and I. Kovalenko, *East.-Eur. J. Enterp. Technol.*, **3**, 56 (2018).